

Searching for Ultralight Dark Matter with Mössbauer Resonance

Peng-Long Zhang,^{1,2} Yu-Ming Yang,^{2,3} Xiao-Jun Bi,^{2,3} Qin Chang,^{1,4} Yu Gao,² Hai-Bo Li,^{2,3} Wei Xu,² and Peng-Fei Yin²

¹*Centre for Theoretical Physics, Henan Normal University, Xinxiang 453007, China*

²*Institute of High Energy Physics, Chinese Academy of Sciences, Beijing 100049, China*

³*School of Physical Sciences, University of Chinese Academy of Sciences, Beijing 100049, China*

⁴*Center for High Energy Physics, Henan Academy of Sciences, Zhengzhou 455004, China*

(Dated: December 23, 2025)

We investigate the feasibility of probing the interaction between ultralight scalar dark matter and atomic nuclei using a stationary Mössbauer spectroscopy scheme. The exceptional energy resolution of the Mössbauer resonance enables testing nuclear energy shifts arising from the local dark matter field. In principle, a stationary measurement allows faster data acquisition and becomes advantageous at higher dark-matter masses in the range 10^{-15} – 10^{-8} eV. We present the projected sensitivity to the dark matter parameter space for three candidate Mössbauer isotopes, ^{109}Ag , ^{45}Sc , and ^{67}Zn . Among them, ^{109}Ag provides the highest sensitivity, followed by ^{67}Zn . For ^{109}Ag , the scalar dark-matter–photon coupling f_γ^{-1} can be constrained down to the level of 10^{-18} GeV^{-1} , exceeding the sensitivity of several existing experiments. The scalar dark-matter–gluon coupling f_g^{-1} can be probed down to 10^{-21} GeV^{-1} , while the scalar dark-matter–quark coupling y_d can reach approximately 10^{-22} GeV^{-1} . These results demonstrate that Mössbauer-based techniques offer a promising and competitive approach for probing ultralight dark matter interactions with Standard Model particles.

I. INTRODUCTION

Understanding the fundamental nature of dark matter remains one of the most profound open questions in modern physics. Although dark matter constitutes approximately 26.8% of the total energy density of the Universe—making it roughly five times more abundant than ordinary (baryonic) matter [1]—its microscopic properties and interactions continue to evade detection. The evidence for dark matter primarily arises from its gravitational effects on galactic and cosmological scales [1–6], yet all attempts to directly observe its non-gravitational interactions with Standard Model particles have so far yielded null results.

Among the wide landscape of dark matter candidates, ultralight dark matter (ULDM) has attracted increasing attention. This class of models postulates bosonic fields with masses spanning a wide range, from $m \sim 10^{-23}$ eV up to 1 eV [7]. In many realizations—such as axions, axion-like particles, and scalar dark matter—the ULDM field behaves as a coherently oscillating classical wave, giving rise to distinctive experimental signatures. These particles often couple feebly to photons, electrons, or nucleons, potentially inducing time-varying fundamental constants or energy-level shifts in atomic and nuclear systems [8–17].

The Mössbauer effect [18] is famous for its exceptional energy resolution in recoil-free nuclear gamma-ray resonance. It can be sensitive to tiny shifts in nuclear transition energy if the nucleus is coupled to a time-variant dark matter field. Such couplings can induce slight but measurable changes in nuclear binding energies, leading to shifts in the resonance lines of the Mössbauer spectrum. The magnitude of these shifts depends solely on the strength of the new interaction and is unaffected by nuclear moments. We explore the sensitivity of ultralight scalar dark matter search using a recently proposed static scheme [19].

While ^{57}Fe is currently the most used nucleus in Mössbauer spectroscopy, a number of other isotopes are known to exhibit even sharper Mössbauer resonance lines [20]. For instance, the $E_0 = 88$ keV transition in ^{109}Ag has an extremely small natural width Γ_0 and can, in principle, achieve an extraordinarily small fractional linewidth of $\Gamma_0/E_0 \sim 10^{-22}$, enabling unprecedented spectroscopic resolution and has been proposed to detect gravitational effects at small scales [19]. Another promising candidate is ^{45}Sc , which exhibits a nuclear transition at 12.4 keV with an isomeric lifetime of $\tau_0 = 0.47$ s and a natural linewidth of $\Gamma_0 = \hbar/\tau_0 = 1.4$ feV. This corresponds to an extraordinarily high quality factor of $Q = E_0/\Gamma_0 \simeq 10^{19}$. However, unlike some other Mössbauer isotopes, the use of ^{45}Sc is limited by the relatively small branching ratio of the β^- decay of its parent nucleus ^{45}Ca into the excited state relevant for the Mössbauer transition. As a result, the achievable resonant photon flux from a radioactive source is significantly suppressed. Earlier attempts to achieve resonant excitation of ^{45}Sc at third-generation synchrotron radiation facilities were therefore unsuccessful due to insufficient spectral flux. This limitation has only recently been overcome with the advent of narrow-band, high-repetition-rate X-ray free-electron lasers (XFELs), most notably the European XFEL [21–23], next generation facilities such as the Shanghai High Repetition Rate XFEL and Extreme Light Facility (SHINE) [24–26], the Shenzhen Superconducting Soft X-ray Free Electron Laser (S³FEL) [27, 28], etc.

These facilities are expected to provide high-brightness, high-repetition-rate X-ray beams suitable for resonant nuclear excitation.

The 93-keV transition in ^{67}Zn , with a fractional linewidth of $\Gamma_0/E_0 \sim 10^{-15}$ [29], has also been successfully employed in high-resolution Mössbauer spectroscopy, particularly for gravitational redshift experiments [30, 31]. We investigate projected sensitivity with Mössbauer measurement employing ^{109}Ag , ^{45}Sc , and ^{67}Zn as candidate isotopes to probe shifts of nuclear transition energy induced by ULDM through recoil-free photons. Key nuclear parameters of these isotopes are summarized in Table I, including the transition energy (E_0), natural linewidth (Γ_0), fractional linewidth (Γ_0/E_0), natural lifetime, experimentally achieved resonance width (Γ_{exp}), and the radioactive parent nuclear lifetime.

Isotope	Nuclear transition energy E_0 (keV)	Natural Width Γ_0 (eV)	Γ_0/E_0	Lifetime	Γ_{exp} (eV)	Parent lifetime (day)
^{109}Ag	88	2.3×10^{-17}	1.2×10^{-22}	27.6 s	1.9×10^{-16}	461 (^{109}Cd)
^{45}Sc	12.4	1.4×10^{-15}	1.1×10^{-19}	0.47 s	7.0×10^{-13} [32]	163 (^{45}Ca)*
^{67}Zn	93.3	5.0×10^{-11}	5.4×10^{-16}	6.4 μs	7.5×10^{-11} [33]	3.3 (^{67}Ga)

TABLE I: Properties of selected Mössbauer isotopes ^{109}Ag , ^{45}Sc , and ^{67}Zn , including nuclear transition energy E_0 , natural linewidth Γ_0 , the ratio Γ_0/E_0 , natural lifetime, experimentally achieved resonance width Γ_{exp} , and the radioactive parent nucleus lifetime. The experimentally achieved resonance widths for ^{45}Sc and ^{67}Zn are adopted from observations. For ^{109}Ag , we assume 1.9×10^{-16} eV for an estimate [19]. * Spontaneous $^{45}\text{Ca} \rightarrow ^{45}\text{Sc}$ decay has a major branching fraction suppression $\mathcal{O}(10^{-5})$ to the first ^{45}Sc excited state, and here we list ^{45}Sc as a candidate due to recent success at XFELs.

II. DARK MATTER INDUCED ENERGY SHIFT

In the ultralight bosonic dark matter scenario, the galactic dark matter behaves as a coherently oscillating classical scalar field with a central frequency set by the nonrelativistic particle energy $\omega_\phi = m_\phi + \mathcal{O}(\beta^2)$ and correspondingly a quite small energy dispersion $\sigma(\omega) \sim \beta^2 m_\phi$. Within one coherent time scale, the local dark matter field value can be written as

$$\phi(t, \vec{x}) \simeq \frac{\sqrt{2\rho_{\text{DM}}}}{m_\phi} \cos\left(\omega_\phi t - m_\phi \vec{\beta} \cdot \vec{x}\right), \quad (1)$$

where $\rho_{\text{DM}} \sim 0.4 \text{ GeV}/(\text{cm})^3$ is the local dark matter density and $|\beta| \sim 10^{-4}$ is the virial velocity, and $\omega_\phi \approx m_\phi$. The shift of the nuclear transition energy induced by dark matter is proportional to the dark matter field. Thus, the energy-level shift of the emitter at position $\vec{x} = \vec{0}$ at time t is $\kappa\phi(t, \vec{0})$. When the photon reaches the absorber located at $\vec{x} = \vec{L}$, the corresponding shift is $\kappa\phi(t+L, \vec{L})$. The resulting difference between the emitter and absorber transition energies is given by

$$\begin{aligned} \Delta E &= \kappa\phi(t+L, \vec{L}) - \kappa\phi(t, \vec{0}) \\ &= \kappa \frac{\sqrt{2\rho_{\text{DM}}}}{m_\phi} \cos\left(\omega_\phi(t+L) - m_\phi \vec{\beta} \cdot \vec{L}\right) - \kappa \frac{\sqrt{2\rho_{\text{DM}}}}{m_\phi} \cos\left(\omega_\phi t - m_\phi \vec{\beta} \cdot \vec{0}\right) \\ &= -2\kappa \frac{\sqrt{2\rho_{\text{DM}}}}{m_\phi} \sin\left(\frac{m_\phi L(1-\beta)}{2}\right) \sin\left(m_\phi \left[t + \frac{L(1-\beta)}{2}\right]\right). \end{aligned} \quad (2)$$

In a Mössbauer measurement, the tiny energy shift we predict can be resolved with exquisite precision.

III. THE STATIONARY SCHEME

To probe potential variations in nuclear transition energies induced by an oscillating dark matter background, we consider a static measurement proposal for the ultra-sharp Mössbauer isotopes [19]. A fixed baseline is introduced between the emitter and the absorber. As the dark matter field modulates the transition energies of both the emitter and absorber, resonant absorption occurs only when the energy of the emitted photon matches the altered nuclear energy level of the absorber. By arranging multiple absorbers at different vertical positions relative to the emitter, the system becomes sensitive to small energy shifts. The location along the vertical axis where resonant absorption is

maximized thus provides a direct measurement of the energy variation, allowing us to infer the influence of the dark matter field on nuclear properties.

As illustrated in Fig. 1, the distance between the emitter and the absorber is denoted by L , while the absorber and the detector are arranged along the vertical direction. If a photon emitted by the source is not resonantly absorbed by the absorber, it passes through and is recorded by the photon detector. Owing to the gravitational redshift induced by the Earth's gravitational potential, a vertical displacement of the photon leads to a shift in its energy. At a specific height, this energy shift can bring the photon into resonance with the absorber, thereby enabling resonant absorption.

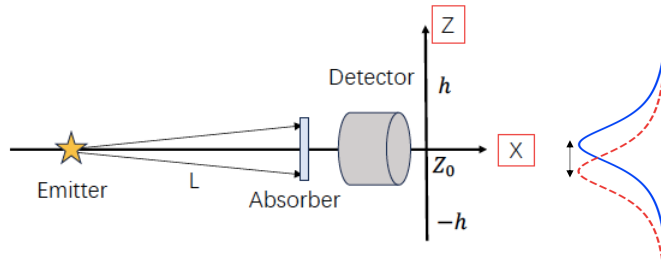


FIG. 1: Illustration for a vertical shift in resonance location.

Let us assume that the emitter is stationary at a vertical position Z_s . The emission line of the source is narrow and unsplit, with a natural linewidth Γ . The measured spectral lineshape is Lorentzian, centered at a resonance energy E_0 . Denoting the total photon emission rate of the source as \dot{N}_0 , the differential number of recoil-free photons with energy E_γ emitted per unit energy and time is given by:

$$\frac{dN_{\text{RF}}(E)}{dE dt} = \dot{N}_0 f_S \cdot \frac{\Gamma/2\pi}{[E - E_0]^2 + (\Gamma/2)^2}, \quad (3)$$

where f_S is the recoil-free fraction of the source emission.

To achieve the desired performance in a static configuration, the detector must have a good spatial resolution, while the finite sizes of the absorber and detector should allow them to cover a narrow vertical range. Within this configuration, the Mössbauer transmission function can be formulated by replacing the conventional Doppler shift with a gravitationally induced energy correction arising from the vertical displacement. The transmission function $C(Z)$ at a detector height Z is:

$$C(Z) = \dot{N}_0 e^{-\mu_e t'} \cdot \left[(1 - f_S) + \int_{-\infty}^{\infty} f_S \xi(Z_S, E_0) \cdot e^{-t \xi(Z, E_0 + \Delta E_0) \Gamma / 2\pi} dE \right], \quad (4)$$

$$\xi(Z, E_0) \equiv \frac{\Gamma/2\pi}{[E - g(Z - Z_S)E - E_0]^2 + (\Gamma/2)^2}.$$

Here, ΔE_0 represents the intrinsic energy offset between the emitter and absorber, which can be compensated by a small vertical height difference within the range of the detector. At resonance, this correction satisfies $g \langle Z - Z_S \rangle E = -\Delta E_0$, and we define the corresponding central detection height as $Z_0 = \langle Z \rangle$ for convenience. The attenuation factor $e^{-\mu_e t'}$ accounts for non-resonant absorption, where t' is the absorber thickness a.k.a. the area density, and μ_e is the mass absorption coefficient at resonance. The effective resonant optical depth is $t = f_A N_M \sigma_0$, where f_A is the recoil-free fraction at the absorber, N_M is the number of Mössbauer nuclei per unit area (which grows with absorber thickness), and σ_0 is the peak resonant cross section.

For practical calculations, the transmission function can be approximated by a simplified parameterization that highlights the gravitational energy shift [19]:

$$C(Z) = \dot{N}_0 e^{-\mu_e t'} \left\{ 1 - f_S \epsilon \cdot \frac{\Gamma_{\text{exp}}^2}{[g(Z - Z_0)E_0]^2 + \Gamma_{\text{exp}}^2} \right\}. \quad (5)$$

Here, ϵ is the effective resonant absorption fraction, and Γ_{exp} is the observed linewidth after transmission through the absorber. Both quantities depend nontrivially on the thickness of the absorber. The quantity f_S represents the fraction of recoil-free emission, while $f_S \epsilon$ represents the total recoil-free absorption fraction.

We consider a factor that induces a frequency shift $\Delta f(t)$ in the resonant absorption of photons by the absorber. This shift results in a vertical displacement of the resonance position, given by

$$Z_0 \rightarrow Z_0(t) = Z_0 + g^{-1} \frac{\Delta f(t)}{f_\gamma}. \quad (6)$$

We define the displacement as $\Delta Z_0(t) \equiv Z_0(t) - Z_0$. This spatial shift can be inferred from variations in Mössbauer absorption efficiency at the detector. If the spatial resolution is sufficiently high, both $\Delta Z_0(t)$ and the corresponding $\Delta f(t)$ can be measured with a sensitivity exceeding the effective Mössbauer linewidth, Γ_{exp}/E_0 .

IV. DRAK MATTER SIGNAL

The interaction between oscillating dark matter and atomic nuclei can induce tiny shifts in nuclear energy levels. This, in turn, causes a slight change in the resonance absorption energy observed in the Mössbauer effect, leading to a vertical displacement of the absorber's resonance absorption position, denoted as $Z_0(t) - Z_0$. This vertical displacement, ΔZ_0 , is quantitatively related to the shift in resonance energy ΔE through the following relation:

$$\delta Z_0 \equiv Z_0(t) - Z_0 = g^{-1} \frac{\Delta f(t)}{f_\gamma} = g^{-1} \frac{\Delta E}{E_0}. \quad (7)$$

The 88 keV emission line of ^{109}Ag has a natural linewidth of 1.1×10^{-17} eV [20, 33]. When both emission and absorption processes are considered, the ideal resonance width effectively doubles. This ^{109}Ag linewidth corresponds to a vertical displacement of about $20 \mu\text{m}$ in Earth's gravitational field with $g = 9.8 \text{ m/s}^2$. To ensure precise localization, the detector is designed with a spatial resolution of $10 \mu\text{m}$, which is half the broadened absorption peak width. We further assume that the detector maintains a high efficiency, approaching 100%, for detecting these high-energy X-ray photons.

The strength of resonance is determined by measuring the unabsorbed photon flux through an absorber layer at height Z . The absorption fraction is given by Eq. 5, and we need to evaluate the statistical significance of measuring the spatial position of the resonance peak. We divide the detector vertically into several bins, each with a height of δZ . The photon flux delivered by the source to the i -th bin, representing the number of photon arrivals per unit time, is denoted as C_i . Far from the resonance point, the photon flux remains unaffected by resonance absorption, so we define this unperturbed arrival rate as C_∞ . For a given Mössbauer source, we set the bin width to match its effective height spread in the local gravitational field. Specifically, we define the bin width is $0.5g^{-1}\Gamma_{\text{exp}}/E_0$. For ^{109}Ag , we choose a bin width of $10 \mu\text{m}$.

Since C_i depends on the parameter Z_0 , the optimal value of Z_0 is determined by minimizing the χ -square function:

$$\chi^2(Z_0) = \sum_i \frac{(C_i(Z_0) - C_i^{\text{exp}})^2}{\Delta_i^2}, \quad (8)$$

which corresponds to a maximum likelihood estimation under the assumption of Gaussian statistical errors. The spatial resolution in determining Z_0 can then be inferred from the sensitivity of the likelihood function to shifts in Z_0 . In the statistics-dominated regime, the uncertainty in each bin is approximated by $\Delta_i = \sqrt{C_i}$.

We numerically simulate the position resolution of the Lorentzian peak, as show-cased in Fig. 2. For ^{109}Ag , the experimental peak width is $20 \mu\text{m}$, and the bin width along the z -axis is $10 \mu\text{m}$. Each bin assumes a number of incident 88 keV photons determined by the intensity and distance of the source. The recoil-free fraction is set to $f_S = 0.5$, and the absorption fraction is $\epsilon = 0.8$. The photon flux measured in the resonance bins decreases due to resonance absorption, as shown by the simulated photon counts in Fig. 2.

For our analysis, we assume that the absorbers and detectors are uniformly arranged on a circle, with the radioactive emitter placed at the geometric center. The angular coverage θ corresponding to the vertical height difference ΔZ_0 of the resonant absorption peaks on the detector is given by

$$\theta = \arctan\left(\frac{\Delta Z_0}{L}\right), \quad (9)$$

where L is the distance between the source and the absorber. In our setup, we take $L = 1 \text{ m}$. For a circular detector geometry, the fraction of the total solid angle subtended by the detector is given by

$$f_\theta = \frac{2\pi\theta}{4\pi} = \frac{\theta}{2}. \quad (10)$$

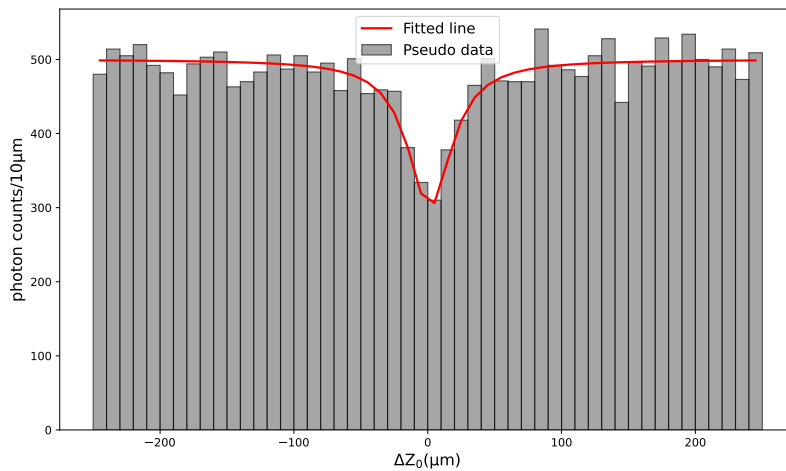


FIG. 2: For the ^{109}Ag nucleus: Simulated peak position accuracy ΔZ_0 obtained from a single pseudo-experiment measuring the position of the absorption Lorentzian peak, assuming an experimental linewidth of $20\ \mu\text{m}$, z -axis bin width of $10\ \mu\text{m}$, 500 arriving photons per bin, recoil-free fraction $f_S = 0.5$, and absorption fraction $\epsilon = 0.8$.

This quantity represents the effective detection solid-angle coverage normalized to the full 4π steradians.

We consider a radioactive source with an activity of $A = 0.1\ \text{Ci}$ (corresponding to $3.7\ \text{GBq}$). The total number of emitted photons during the measurement is

$$N_{total} = A \times P_\gamma \times f_{BR} \times \Delta t \times N_{exp}, \quad (11)$$

where $P_\gamma = 1/(1 + \alpha_T)$ is the probability of photon emission, α_T is the internal conversion coefficient, defined as the ratio between the number of internal conversion electrons N_{IC} and the number of gamma emissions N_γ , f_{BR} denotes the branching ratio for the transition of interest, $\Delta t = T/3$ is the integration time per data segment, with $T = h/m_\phi$ being the oscillation period associated with dark matter of mass m_ϕ , and h the Planck constant, $N_{exp} = 10^6$ accounts for the statistical enhancement from the number of DM periods during its coherent time scale, which we take as one single data taking period. We will take the DM coherent time scale $t_c = N_{exp} \cdot 2\pi m_\phi^{-1}$ as the benchmark coherent measurement time in this sensitivity estimate, and longer time data-taking would be considered as repeated yet independent measurements. For each energy bin, the number of photons contributing to that bin is

$$N_\gamma = N_{total} \times f_\theta. \quad (12)$$

This framework provides a quantitative estimate of the photon statistics available per bin under realistic experimental conditions, which is crucial for determining the achievable sensitivity of the measurement.

For ^{45}Sc , two approaches can be employed to generate Mössbauer radiation. The conventional route assumes a radioactive ^{45}Ca source with an activity of $0.1\ \text{Ci}$. However, directly using ^{45}Ca is inefficient as they almost always decay to the ground state of ^{45}Sc . An alternative approach relies on synchrotron radiation to resonantly excite the ^{45}Sc nucleus, for instance, by a high-intensity X-ray beam [34]. The resonance excitation of ^{45}Sc by XFEL beam generates coherently scattered photons in the forward direction [35]. The yield of pure nuclear-resonant photons can be estimated from the incident photon flux within the narrow resonance bandwidth. Owing to the relatively long lifetime of ^{45}Sc ($0.47\ \text{s}$), the nuclear-resonant signal can be effectively distinguished from the directly transmitted incident beam. The beam-excited Mössbauer resonance photon flux N_γ^{MS} can be estimated as

$$N_\gamma^{\text{MS}} = N_\gamma^{\text{SR}} \frac{\Gamma}{\Delta E^{\text{SR}}}, \quad (13)$$

where N_γ^{SR} denotes the spectral photon flux of the synchrotron radiation, Γ is the natural linewidth of the ^{45}Sc nuclear transition, and ΔE^{SR} represents the energy resolution of the synchrotron source. We adopt $\Delta E^{\text{SR}} = 1\ \text{meV}$ for a modern SR source such as the European XFEL [21–23]. These resonance photons are typically pointed in angular direction, and in principle can be more efficiently covered by detectors. Under these circumstances, we make a simple assumption that the majority of such Mössbauer photons by synchrotron radiation can be received by the absorber or the detector. Accordingly, the number of photons N_γ reaching the absorber in each energy bin can be estimated as

$$N_\gamma = N_\gamma^{\text{MS}} \times P_\gamma \times \Delta t \times N_{exp}. \quad (14)$$

In the following analysis, we consider a spectral photon flux of $N_\gamma^{\text{SR}} = 1 \times 10^{12} \text{ ph s}^{-1} \text{ meV}^{-1}$ [21].

To ensure that the signal-to-noise ratio reaches the level of at least 3σ , the numbers of detected signal and background events must satisfy:

$$\frac{N_S}{\sqrt{N_S + N_B}} \geq 3\sigma, \quad (15)$$

where N_S denotes the number of signal events and is given by $N_S = \epsilon f_S N_\gamma$. The remaining events are treated as background, so the background count is $N_B = N_\gamma - N_S$. Substituting these expressions into Eq. (15) and solving for the total number of detected photons N_γ , we obtain the minimal number of photons required to achieve a 3σ detection significance:

$$N_\gamma \geq \left(\frac{3\sigma}{\epsilon f_S} \right)^2. \quad (16)$$

This condition sets a lower bound on the total number of photons that must be collected in order for the signal to be statistically distinguishable from the background at the desired confidence level.

Generally, one needs to balance a larger absorption fraction against the mass attenuation. Reference [36] showed that a mass attenuation near $\mu_e t' \approx 2$ provides the best sensitivity, with a corresponding absorber efficiency of $\epsilon \approx 0.8$ [19]. For ^{109}Ag recoil-free fraction $f_S = 0.05$ [37], and the absorption fraction $\epsilon = 0.8$. We use the χ -square formula to determine the fitted ΔZ_0 value. The fit for one simulation is presented in Fig. 2. We then perform 1000 simulation runs to obtain the 95% confidence interval for ΔZ_0 .

We extend the methodology previously applied to the ^{109}Ag nucleus to two additional emitters: ^{45}Sc and ^{67}Zn . For ^{45}Sc , the 12.4 keV nuclear transition has an intrinsic experiment linewidth of $7.0 \times 10^{-13} \text{ eV}$ [32], which corresponds to a vertical energy shift of approximately $\delta Z = 0.52 \text{ m}$ in Earth's gravitational field. To resolve this gravitationally induced broadening, the detector is designed with a spatial resolution of 0.26 m, i.e., half the broadened absorption width. For ^{67}Zn , the 93.3 keV transition has a much larger experiment linewidth of $7.5 \times 10^{-11} \text{ eV}$ [33], resulting in a gravitational broadening of $\delta Z = 7.4 \text{ m}$; accordingly, the detector spatial resolution is set to 3.7 m. The Lamb-Mössbauer factors at room temperature, estimated within the Debye approximation, are approximately 0.75 [21] for ^{45}Sc and 0.2 [38] for ^{67}Zn , respectively. In both cases, we employ a χ^2 -minimization procedure to extract the best-fit vertical displacement Z_0 . Based on 1000 Monte Carlo simulations, we determine the 95% confidence intervals of ΔZ_0 for ^{45}Sc and ^{67}Zn .

In Table II, we summarize the key nuclear parameters of these isotopes, including internal conversion coefficient α_T [39], probability of gamma P_γ , branching ratio f_{BR} [39], recoil-free fraction f_S , and the absorption fraction ϵ is taken to be 0.8.

Isotope	α_T	P_γ	f_{BR}	f_S
^{109}Ag	26.3	0.037	1	0.05
^{45}Sc	423	0.0024	2×10^{-5}	0.75
^{67}Zn	0.873	0.534	0.52	0.2

TABLE II: Properties of selected Mössbauer isotopes ^{109}Ag , ^{45}Sc , and ^{67}Zn , including internal conversion coefficient α_T , probability of gamma P_γ , branching ratio f_{BR} , recoil-free fraction f_S , and the absorption fraction $\epsilon = 0.8$ throughout.

V. DARK MATTER - NUCLEUS INTERACTIONS

In this section, we explore how dark matter interactions with photons, quarks, and gluons can affect the energy levels of atomic nuclei. We will present the corresponding Lagrangians for each type of interaction and derive the formulas for the resulting energy shifts in the nuclei.

To describe the interaction between the ultra-light dark matter (ULDM) field ϕ and the Standard Model, we consider a linear coupling of ϕ to quarks (q), gluons ($G_{a\mu\nu}$), and photons ($F_{\mu\nu}$). The corresponding interaction Lagrangian takes the form [33]:

$$\mathcal{L} \supset -y_q \phi \bar{q} q - \frac{\alpha \phi}{4 f_\gamma} F^2 - \frac{\beta(\alpha_s)}{4\alpha_s} \frac{\phi}{f_g} G^2, \quad (17)$$

where, $G^2 = G_{\mu\nu}^a G^{a\mu\nu}$ with a being the color index, $F^2 = F_{\mu\nu} F^{\mu\nu}$, y_q , f_γ and f_g denotes the interaction strength with various modules.

These interactions can induce time-dependent variations in fundamental constants such as the fine-structure constant α , the down quark, and the QCD structure constant α_s . Such variations lead to shifts in nuclear energy levels, which can be estimated for each type of coupling.

Photon coupling: The term $\frac{\alpha\phi}{4f_\gamma}F^2$ leads to a change in the fine-structure constant, $\Delta\alpha/\alpha \simeq -\alpha\phi/f_\gamma$, which alters the electromagnetic self-energy of the nucleus. For a nucleus with Z protons and mass number A , the resulting energy shift is approximately [33]

$$\Delta E \simeq -\frac{Z\alpha^2}{A^{1/3}r_0} \frac{\Delta\phi}{f_\gamma}, \quad (18)$$

where $r_0 \approx 1.2$ fm is a typical nuclear scale.

Quark (Yukawa) coupling: As an example of the Yukawa couplings in Eq. 17, we focus on the scalar field ϕ coupling to the down quark through the interaction term $y_d \bar{d}d$. To estimate the resulting shift in nuclear energy levels induced by ϕ , we consider the change in the one-pion-exchange potential and equate it to the energy shift ΔE , yielding [33, 40]

$$\Delta E \simeq 2.5 y_d \Delta\phi. \quad (19)$$

Gluon coupling: The coupling $\frac{\beta(\alpha_s)}{4\alpha_s} \frac{\phi}{f_g} G^2$ shifts the QCD structure constant. The induced energy shift is approximately [33]

$$\Delta E \simeq 0.08 \text{ GeV} \frac{\Delta\phi}{f_g}. \quad (20)$$

VI. PROJECTED SENSITIVITY

We investigate the parameter space for each interaction channel by equating the dark matter-induced energy shifts, given in Eqs. 18, 19, and 20, to the experimentally accessible shift described in Eq. 7. An emitter source with an activity of $A = 0.1$ Ci (3.7 GBq) is located at the center, while the absorber and detectors are uniformly distributed along a circle of radius $L = 1$ m for ^{109}Ag and ^{45}Sc , and $L = 50$ m for ^{67}Zn . Under these conditions, we derive the corresponding constraints on the DM-photon coupling constant f_γ are presented in Fig.3, the DM-gluon coupling constant f_g are presented in Fig.4a, and the DM-quark coupling constant y_d are presented in Fig.4b, at the 95% confidence level. In our analysis, we adopt the parameters listed in Table I and Table II. For the traditional Mössbauer sources based on ^{109}Ag , ^{45}Sc , and ^{67}Zn , the experimentally measured linewidths are used in the transmission function given in Eq. 5. For the Mössbauer resonance of ^{45}Sc excited by synchrotron radiation, the nuclear resonance photon flux N_γ^{MS} in Eq. 13 is calculated using the natural linewidth, while the experimentally measured linewidth is adopted in the transmission function Eq. 5.

Figure 3 shows the constraints on the scalar DM-photon coupling f_γ^{-1} . The red dashed line corresponds to ^{109}Ag , the black dashed line to ^{45}Sc with a radioactive source, the black dot-dashed line to ^{45}Sc with synchrotron radiation, and the blue dashed line to ^{67}Zn with a baseline of 50 m. The applicable dark matter range is truncated by requiring the dark matter coherent time not exceeding the decay lifetime of the parent isotope (low frequency), and the 3σ statistic requirement of sufficient photon counts in each height bin (high frequency). While the SR scenario is not subject to the parent's decay lifetime, it should observe realistic operation time limits at a facility. For observation time, we take one coherent time of dark matter, $\tau = 10^6 \cdot 2\pi m_\phi^{-1}$, which is already a significant time duration in the relatively low dark matter mass range. At high dark matter masses, longer observation time periods $t_{\text{obs}} \gg t$ can yield repeated and independent measurements, and improve the sensitivity statistically. For ^{109}Ag , a projected sensitivity at the level of $10^{-18} - 10^{-17} \text{ GeV}^{-1}$ can be achieved in the DM mass region $10^{-15} - 10^{-11} \text{ eV}$. For ^{67}Zn , the coupling can be constrained at the level of $10^{-16} - 10^{-13} \text{ GeV}^{-1}$ in the dark matter mass region $10^{-13} - 10^{-8} \text{ eV}$. For ^{45}Sc , the traditional radioactive source yields a sensitivity of approximately $10^{-14} - 10^{-12} \text{ GeV}^{-1}$ in the dark matter mass range $10^{-14} - 10^{-9} \text{ eV}$, while the synchrotron radiation based source achieves a sensitivity of about $10^{-13} - 10^{-12} \text{ GeV}^{-1}$ in the dark matter mass range $10^{-15} - 10^{-13} \text{ eV}$.

In Fig. 3, the green region indicates the GEO 600 bound [41], obtained through spectral analysis of the strain data from the GEO 600 gravitational-wave interferometer. The magenta region shows the exclusion limit from Dynamical Decoupling (DD) [42], derived from the non-observation of variations in the fine-structure constant α caused by oscillating scalar dark matter in an atomic optical transition. The cyan region represents the 'Dark Matter from Non Equal Delays' experiment bound [43], obtained from searches for dark matter using an optical cavity with unequal

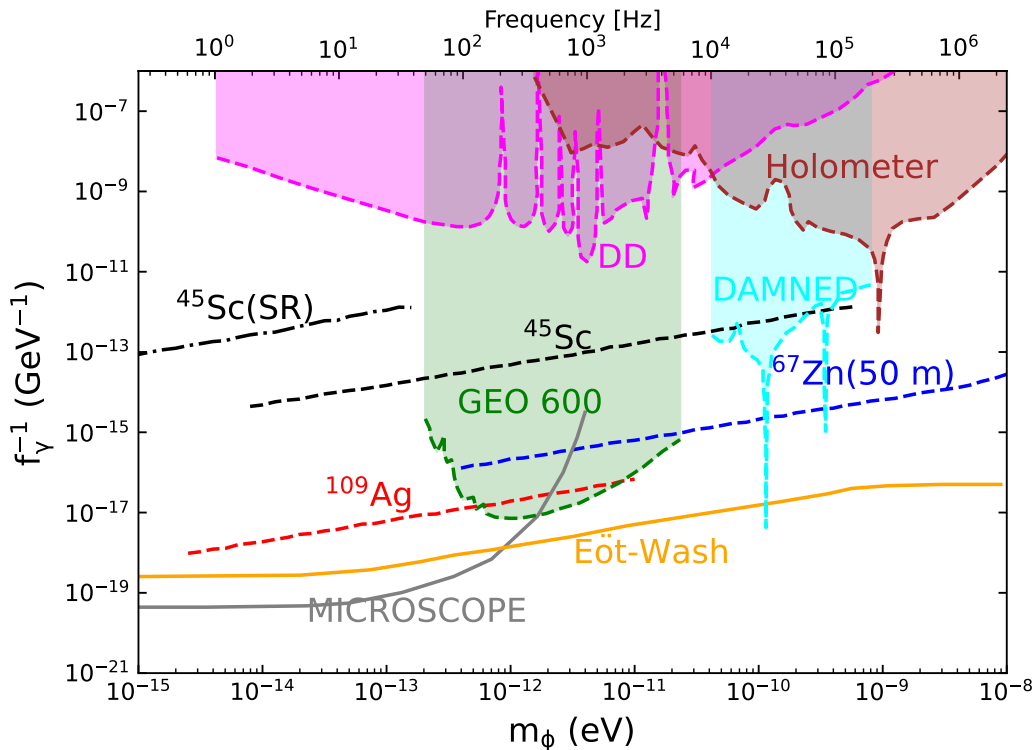


FIG. 3: Projected sensitivity to the scalar DM–photon coupling f_γ^{-1} versus the dark matter mass m_ϕ . Time exposure assumes one dark matter coherent time, $t_c = 10^6 \cdot 2\pi m_\phi^{-1}$. Red, black, and blue dashed lines denote results for ^{109}Ag , ^{45}Sc and ^{67}Zn , respectively, while the black dot-dashed line corresponds to ^{45}Sc (SR) with synchrotron radiation. Existing constraints from GEO 600 [41], DD [42], DAMNED [43], Holometer [44], as well as equivalence-principle tests by MICROSCOPE [45, 46] and Eöt-Wash [47, 48], are shown for comparison. For ^{109}Ag , ^{45}Sc , and ^{67}Zn using traditional radioactive sources, the source activity is fixed at 0.1 Ci. For ^{45}Sc with synchrotron radiation (SR), a spectral photon flux of $1 \times 10^{12} \text{ ph s}^{-1} \text{ meV}^{-1}$ is assumed. The baseline distance is 1 m for ^{109}Ag and ^{45}Sc , and 50 m for ^{67}Zn .

delay interferometry. The brown region shows the Holometer bound [44], derived by studying variations of the fine-structure constant α using cross-correlated data from the Fermilab Holometer instrument. The solid gray lines and the solid orange line represent constraints from “fifth-force” (FF) searches and tests of the equivalence principle (EP). The most stringent constraints for this dark matter scenario come from the MICROSCOPE experiment [45, 46], indicated by the solid gray lines, and the Cu/Pb torsion pendulum experiment performed by the Eöt-Wash group [47, 48], indicated by the solid orange line, as computed in Refs. [16, 49]. Among the three nuclei, ^{109}Ag exhibits the strongest sensitivity, followed closely by ^{67}Zn , while the constraint obtained from ^{45}Sc is comparatively weaker. The results based on ^{109}Ag and ^{67}Zn provide constraints that are stronger than those obtained by the DD, DAMNED, Holometer. The constraint derived from ^{109}Ag is at a sensitivity level comparable to that achieved by the GEO 600 experiments, whereas the constraint from ^{67}Zn is weaker than that of GEO 600. Although the ^{109}Ag result does not surpass the limits from equivalence-principle (EP) violation tests, it approaches a similar order of magnitude in sensitivities over certain dark matter ranges.

Similarly, the projected sensitivity can be estimated for dark matter couplings to gluons and quarks. These sensitivities are calculated for one type of coupling in each plot, ignoring potential interferences. Figure 4a shows the constraints on the scalar DM–gluon coupling f_g^{-1} . The strongest limits are obtained from ^{109}Ag , for which f_g^{-1} reaches the $10^{-21} \text{ GeV}^{-1}$ level, followed closely by ^{67}Zn , while the constraint derived from ^{45}Sc is comparatively weaker. Figure 4b presents the constraints on the scalar DM–quark coupling y_d . Again, ^{109}Ag provides the most stringent bounds, reaching the $10^{-22} \text{ GeV}^{-1}$ level, followed by ^{67}Zn , with ^{45}Sc yielding weaker constraints.

Among the three nuclei considered ^{109}Ag , ^{45}Sc and ^{67}Zn , ^{109}Ag yields the strongest constraints on the dark matter couplings, making it the most promising candidate for future precision experiments aimed at probing interactions between dark matter and the Standard Model. The second strongest constraints are obtained from ^{67}Zn with a baseline of $L = 50 \text{ m}$, while ^{45}Sc with a traditional radioactive source provides comparatively weaker limits. Although

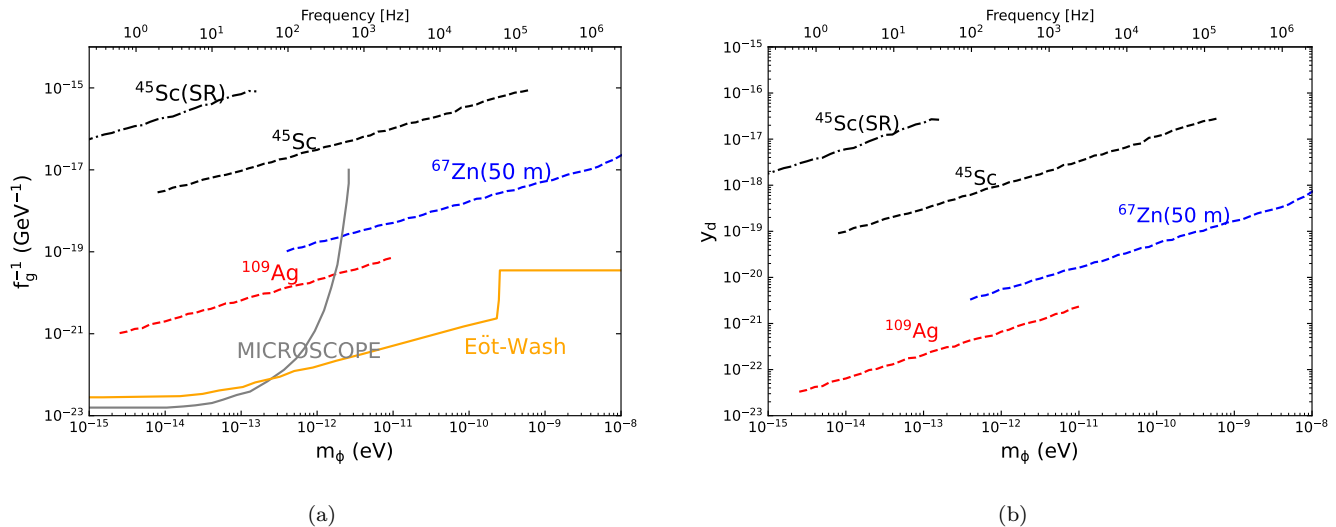


FIG. 4: Projected sensitivity to the scalar DM-gluon coupling f_g^{-1} (a) and the scalar DM-quarks coupling y_d (b), versus the dark matter mass m_ϕ . Red, black, and blue dashed lines denote results for ^{109}Ag , ^{45}Sc and ^{67}Zn , respectively, while the black dot-dashed line corresponds to ^{45}Sc with synchrotron radiation. Existing constraints from equivalence-principle tests by MICROSCOPE [45, 46] and Eöt-Wash [47, 48] are shown for comparison.

the current constraints derived from ^{45}Sc using a synchrotron-radiation-based source are weaker than those obtained from the other nuclei, this approach offers several important advantages. In particular, the experimental integration time can be extended, and the photon flux may be significantly improved with future advances in synchrotron technology. An X-ray free-electron laser oscillator represents a promising next-generation hard X-ray source, capable of delivering fully coherent pulses with meV-level bandwidth and a highly stable flux that is expected to reach $1 \times 10^{15} \text{ ph s}^{-1} \text{ meV}^{-1}$ [50]. If applied to dark matter searches, such improvements would substantially increase the number of available photons and could further enhance the experimental sensitivity. Overall, ^{109}Ag provides the most stringent and robust constraints among the nuclei considered, highlighting its strong potential for future high-precision probes of dark-matter interactions with the Standard Model.

VII. CONCLUSIONS

The Mössbauer effect is a powerful tool for detecting small shifts in nuclear energy levels. In this study, we explore its potential for probing the coupling between dark matter and nuclei in the source and absorber of a Mössbauer spectrometer. To investigate possible variations in nuclear transition energies induced by an oscillating dark matter background, we consider a static Mössbauer measurement scheme to probe nuclear transition energy variations induced by an oscillating scalar dark matter field. The ultralight dark matter interacting with both the emitter and absorber can lead to a variation in their nuclear energy levels, resulting in a measurable shift in the position of the Mössbauer resonance.

In our analysis, we select ^{109}Ag , ^{45}Sc , and ^{67}Zn as candidate Mössbauer isotopes. We assume an emitter source with an activity of $A = 0.1 \text{ Ci}$ (3.7 GBq), and also consider ^{45}Sc with synchrotron radiation scheme. The baseline distance between emitter and absorber for ^{109}Ag , ^{45}Sc is $L = 1 \text{ m}$, for ^{67}Zn is $L = 50 \text{ m}$. The dark-matter mass is varied in the range from 10^{-15} eV to 10^{-8} eV . Under these assumptions, we derive projected constraints on the dark-matter-photon coupling f_γ^{-1} , the dark-matter-gluon coupling f_g^{-1} , and the dark-matter-quark coupling y_d .

Among the three isotopes considered, ^{109}Ag provides the highest sensitivity, followed by ^{67}Zn , while ^{45}Sc yields the lowest sensitivity. For the scalar dark-matter-photon coupling f_γ^{-1} , ^{109}Ag and ^{67}Zn yield constraints that are stronger than those obtained from several existing experiments, such as Dynamical Decoupling, DAMNED, and the Holometer. In particular, the best constraints obtained with ^{109}Ag can reach the level of $10^{-18} \text{ GeV}^{-1}$. For the scalar dark matter-gluon coupling f_g^{-1} , ^{109}Ag can achieve sensitivities down to the level of $10^{-21} \text{ GeV}^{-1}$. For the scalar dark matter-quark coupling y_d , the sensitivity of ^{109}Ag can reach approximately $10^{-22} \text{ GeV}^{-1}$.

In this work, we have considered a table-top baseline distance of $L = 1 \text{ m}$ for ^{109}Ag . In the long DM wavelength limit, extending the baseline to 10 m or 100 m linearly increases the energy shift at the cost of lowering statistics at the

detectors. As the significance depends on photon counting as $\sim 1/\sqrt{N}$, a longer baseline still expects an improvement to the sensitivity. Further enhancements could be achieved by increasing the source activity and incorporating optic control, both of which would increase the number of detected photons and thereby improve the photon statistics.

In light of future powerful synchrotron radiation sources delivering high-brightness X-ray beams, synchrotron-based Mössbauer spectroscopy has become increasingly important. In particular, the development of narrow-band, high-repetition-rate XFELs has enabled resonant excitation of ^{45}Sc , as recently demonstrated at the European XFEL. If such technology were applied to dark matter searches, it could substantially increase the number of emitted photons and further enhance the experimental sensitivity.

ACKNOWLEDGMENTS

The authors thank Hua-Qiao Zhang, Xing-Jian Lv and Han Miao for valuable discussions. This work is supported by the National Natural Science Foundation of China (Grants No. 12175248, No. 12275067, and No. 11947005), Science and Technology R&D Program Joint Fund Project of Henan Province (Grant No.225200810030), Science and Technology Innovation Leading Talent Support Program of Henan Province, and National Key R&D Program of China (Grant No. 2023YFA1606000). During the preparation of this paper, [51] appeared with a focus on the pseudo-scalar type of ultra-light dark matter.

-
- [1] N. Aghanim *et al.* (Planck), *Astron. Astrophys.* **641**, A6 (2020), [Erratum: *Astron. Astrophys.* 652, C4 (2021)], arXiv:1807.06209 [astro-ph.CO].
 - [2] E. Corbelli and P. Salucci, *Mon. Not. Roy. Astron. Soc.* **311**, 441 (2000), arXiv:astro-ph/9909252.
 - [3] D. Clowe, M. Bradac, A. H. Gonzalez, M. Markevitch, S. W. Randall, C. Jones, and D. Zaritsky, *Astrophys. J. Lett.* **648**, L109 (2006), arXiv:astro-ph/0608407.
 - [4] D. Clowe, A. Gonzalez, and M. Markevitch, *Astrophys. J.* **604**, 596 (2004), arXiv:astro-ph/0312273.
 - [5] M. Markevitch, A. H. Gonzalez, L. David, A. Vikhlinin, S. Murray, W. Forman, C. Jones, and W. Tucker, *Astrophys. J. Lett.* **567**, L27 (2002), arXiv:astro-ph/0110468.
 - [6] G. Jungman, M. Kamionkowski, and K. Griest, *Phys. Rept.* **267**, 195 (1996), arXiv:hep-ph/9506380.
 - [7] E. G. M. Ferreira, *Astron. Astrophys. Rev.* **29**, 7 (2021), arXiv:2005.03254 [astro-ph.CO].
 - [8] M. S. Safronova, D. Budker, D. DeMille, D. F. J. Kimball, A. Derevianko, and C. W. Clark, *Rev. Mod. Phys.* **90**, 025008 (2018), arXiv:1710.01833 [physics.atom-ph].
 - [9] D. Antypas, D. Budker, V. V. Flambaum, M. G. Kozlov, G. Perez, and J. Ye, *Annalen Phys.* **532**, 1900566 (2020), arXiv:1912.01335 [physics.atom-ph].
 - [10] T. Damour and A. M. Polyakov, *Nucl. Phys. B* **423**, 532 (1994), arXiv:hep-th/9401069.
 - [11] J. D. Barrow, *Phys. Rev. D* **59**, 043515 (1999).
 - [12] H. B. Sandvik, J. D. Barrow, and J. Magueijo, *Phys. Rev. Lett.* **88**, 031302 (2002), arXiv:astro-ph/0107512.
 - [13] A. Arvanitaki, J. Huang, and K. Van Tilburg, *Phys. Rev. D* **91**, 015015 (2015), arXiv:1405.2925 [hep-ph].
 - [14] Y. V. Stadnik and V. V. Flambaum, *Phys. Rev. Lett.* **115**, 201301 (2015), arXiv:1503.08540 [astro-ph.CO].
 - [15] A. Banerjee, H. Kim, and G. Perez, *Phys. Rev. D* **100**, 115026 (2019), arXiv:1810.01889 [hep-ph].
 - [16] A. Hees, O. Minazzoli, E. Savalle, Y. V. Stadnik, and P. Wolf, *Phys. Rev. D* **98**, 064051 (2018), arXiv:1807.04512 [gr-qc].
 - [17] E. Savalle, B. M. Roberts, F. Frank, P.-E. Pottie, B. T. McAllister, C. Dailey, A. Derevianko, and P. Wolf, (2019), arXiv:1902.07192 [gr-qc].
 - [18] R. L. Mössbauer, *Z. Phys.* **151**, 124 (1958).
 - [19] Y. Gao, H. Zhang, and W. Xu, *Sci. Bull.* **69**, 2795 (2024), arXiv:2310.06607 [gr-qc].
 - [20] M. E. D. Center, Properties of isotopes relevant to mossbauer spectroscopy, <http://www.medc.dicp.ac.cn/Resources.htm> (2025), accessed: 07 11, 2025.
 - [21] Y. Shvyd'ko, R. Röhlberger, O. Kocharovskaya, *et al.*, *Nature* **622**, 471 (2023).
 - [22] W. Decking *et al.*, *Nature Photon.* **14**, 391 (2020).
 - [23] S. Liu, C. Grech, M. Guetg, *et al.*, *Nature Photonics* **17**, 984 (2023).
 - [24] J. Wan, Y. Leng, B. Gao, F. Chen, J. Chen, L. Lai, W. Zhou, and W. Xu, *Nucl. Instrum. Meth. A* **1026**, 166200 (2022).
 - [25] Z.-T. Zhao, C. Feng, and K.-Q. Zhang, *Nucl. Sci. Tech.* **28**, 117 (2017).
 - [26] Z. Zhao, C. Feng, J. Chen, and Z. Wang, *Science Bulletin* **61**, 720 (2016).
 - [27] X. Wang *et al.*, *JACoW IPAC2023*, TUPL043 (2023).
 - [28] Z. Li, J. Shao, H. Qizhang, J. Yang, and W. Zhang, *JACoW LINAC2024*, TUPB048 (2024).
 - [29] D. Griesinger, R. V. Pound, and W. Vetterling, *Phys. Rev. B* **15**, 3291 (1977).
 - [30] T. Katila and K. Riski, *Physics Letters A* **83**, 51 (1981).
 - [31] W. Potzel, C. Schäfer, M. Steiner, *et al.*, *Hyperfine Interact* **72**, 195–214 (1992).
 - [32] P. Liu *et al.*, (2025), arXiv:2508.17538 [quant-ph].
 - [33] G. Gratta, D. E. Kaplan, and S. Rajendran, *Phys. Rev. D* **102**, 115031 (2020), arXiv:2010.03588 [hep-ph].

- [34] Y. Shvyd'ko *et al.*, *Nature* **622**, 471 (2023).
- [35] W. Sturhahn, *Journal of Physics: Condensed Matter* **16**, S497 (2004).
- [36] G. J. Long, T. E. Cranshaw, and G. Longworth, *Mössbauer Effect Reference and Data Journal* **6**, 42 (1983).
- [37] W. Wildner and U. Gonser, *Le Journal De Physique Colloques* **40** (1979).
- [38] W. Potzel, Zinc-67 mössbauer spectroscopy, in *Mössbauer Spectroscopy Applied to Magnetism and Materials Science*, edited by G. J. Long and F. Grandjean (Springer US, Boston, MA, 1993) pp. 305–371.
- [39] <https://www-nds.iaea.org/relnsd/vcharthtml/VChartHTML.html>.
- [40] H. Murayama, Lecture notes on many body problems, <http://hitoshi.berkeley.edu/221B-S01/8.pdf>.
- [41] S. M. Vermeulen *et al.* 10.1038/s41586-021-04031-y (2021), arXiv:2103.03783 [gr-qc].
- [42] S. Aharony, N. Akerman, R. Ozeri, G. Perez, I. Savoray, and R. Shaniv, *Phys. Rev. D* **103**, 075017 (2021), arXiv:1902.02788 [hep-ph].
- [43] E. Savalle, A. Hees, F. Frank, E. Cantin, P.-E. Pottie, B. M. Roberts, L. Cros, B. T. Mcallister, and P. Wolf, *Phys. Rev. Lett.* **126**, 051301 (2021), arXiv:2006.07055 [gr-qc].
- [44] L. Aiello, J. W. Richardson, S. M. Vermeulen, H. Grote, C. Hogan, O. Kwon, and C. Stoughton, *Phys. Rev. Lett.* **128**, 121101 (2022), arXiv:2108.04746 [gr-qc].
- [45] P. Touboul *et al.*, *Phys. Rev. Lett.* **119**, 231101 (2017), arXiv:1712.01176 [astro-ph.IM].
- [46] J. Bergé, P. Brax, G. Métris, M. Pernot-Borràs, P. Touboul, and J.-P. Uzan, *Phys. Rev. Lett.* **120**, 141101 (2018), arXiv:1712.00483 [gr-qc].
- [47] G. L. Smith, C. D. Hoyle, J. H. Gundlach, E. G. Adelberger, B. R. Heckel, and H. E. Swanson, *Phys. Rev. D* **61**, 022001 (2000), arXiv:2405.10982 [gr-qc].
- [48] S. Schlamminger, K. Y. Choi, T. A. Wagner, J. H. Gundlach, and E. G. Adelberger, *Phys. Rev. Lett.* **100**, 041101 (2008), arXiv:0712.0607 [gr-qc].
- [49] H. Banks, E. Fuchs, and M. McCullough, (2024), arXiv:2407.11112 [hep-ph].
- [50] B. Adams *et al.*, (2019), arXiv:1903.09317 [physics.ins-det].
- [51] S. Liu, K.-F. Lyu, J. Meng, J. Shu, Y. Wang, and Y. Zhao, Probing axion via mössbauer spectroscopy (2025), arXiv:2511.14851 [hep-ph].